

Reentrant Phase Behavior in Protein Solutions Induced by Multivalent Salts: Strong Effect of Anions Cl^- Versus NO_3^-

Michal K. Braun,[†] Andrea Sauter,[†] Olga Matsarskaia,[†] Marcell Wolf,^{†,‡} Felix Roosen-Runge,^{‡,§} Michael Sztucki,[§] Roland Roth,^{||} Fajun Zhang,^{*,†} and Frank Schreiber[†]

[†]Institut für Angewandte Physik, Universität Tübingen, Auf der Morgenstelle 10, 72076 Tübingen, Germany

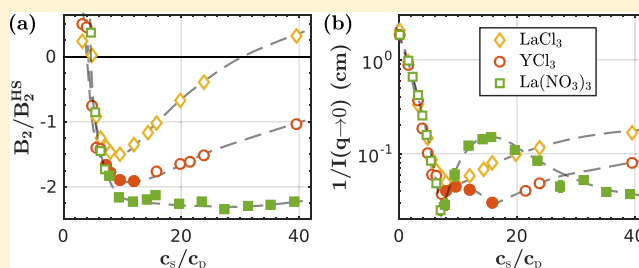
[‡]Division of Physical Chemistry, Department of Chemistry, Lund University, Naturvetarvägen 14, 22100 Lund, Sweden

[§]ESRF—The European Synchrotron Radiation Facility, 71 avenue des Martyrs, 38000 Grenoble, France

^{||}Institut für Theoretische Physik, Universität Tübingen, Auf der Morgenstelle 14, 72076 Tübingen, Germany

Supporting Information

ABSTRACT: In this work, the effects of the two anions Cl^- and NO_3^- on the phase behavior of bovine serum albumin (BSA) in solution with trivalent salts are compared systematically. In the presence of trivalent metal salts, negatively charged proteins such as BSA in solution undergo a reentrant condensation (RC) phase behavior, which has been established for several proteins with chlorides of trivalent salts. Here, we show that replacing Cl^- by NO_3^- leads to a marked change in the phase behavior. The effect is investigated for the two different cations Y^{3+} and La^{3+} . The salts are thus YCl_3 , $\text{Y}(\text{NO}_3)_3$, LaCl_3 , and $\text{La}(\text{NO}_3)_3$. The experimental phase behavior shows that while the chloride salts induce both liquid–liquid phase separation (LLPS) and RC, the nitrate salts also induce LLPS, but RC becomes partial with $\text{La}(\text{NO}_3)_3$ and disappears with $\text{Y}(\text{NO}_3)_3$. The observed phase behavior is rationalized by effective protein–protein interactions which are characterized using small-angle X-ray scattering. The results based on the reduced second virial coefficients B_2/B_2^{HS} and $1/I(q \rightarrow 0)$ demonstrate that the NO_3^- salts induce a stronger attraction than the Cl^- salts. Overall, the effective attraction, the width of the condensed regime in the RC phase diagram, and the nature of LLPS follow the order $\text{LaCl}_3 < \text{YCl}_3 < \text{La}(\text{NO}_3)_3 < \text{Y}(\text{NO}_3)_3$. Despite the decisive role of cations in RC phase behavior, isothermal titration calorimetry measurements indicate that replacing anions does not significantly influence the cation binding to proteins. The experimental results observed are discussed based on an “enhanced Hofmeister effect” including electrostatic and hydrophobic interactions between protein–cation complexes.



INTRODUCTION

The complex interactions between proteins in solution, which lead to a diversified phase behavior, are essential for understanding the physical mechanisms of protein crystallization, protein-condensation-related diseases, and phase transitions in the cell, as well as in pharmaceutical industry.^{1–9}

Proteins are often modeled as small colloidal particles in terms of effective interactions. However, globular proteins typically have both positive and negative charges, complex charge patterns, and hydrophobic patches on the surface, which make effective interactions highly sensitive to environmental parameters.^{2,10–22} One such parameter is the concentration of trivalent salts which have been demonstrated in recent studies to be very efficient in tuning interactions in protein solutions, and an interesting phase behavior has been reported including reentrant condensation (RC),^{23–27} metastable liquid–liquid phase separation (LLPS),^{25,28–32} crystallization,^{25,28,30,33–36} gelation via arrested phase separation, and cluster formation.^{30,37–39}

RC describes a typical phase behavior of protein solutions in the presence of multivalent salts: negatively charged proteins such as bovine serum albumin (BSA) in solution in the presence of trivalent salts, such as YCl_3 , $\text{Y}(\text{NO}_3)_3$, LaCl_3 , and $\text{La}(\text{NO}_3)_3$, form a condensed regime in between two critical salt concentrations $c^* < c^{**}$.^{23–25} The physical mechanism of RC has been demonstrated to be charge inversion of proteins due to cation binding to the carboxyl groups on the protein surface.^{24,26} So far, it has been shown that the RC phase behavior can be manipulated by the type of cations, the solvent isotope (H_2O vs D_2O), as well as the ionic strength of additional co-salts.^{24,27,31,40}

Here, we show that the RC behavior is also remarkably sensitive to the trivalent salt anion. Previous studies have shown that the change from NaCl to NaNO_3 has a rather weak effect on BSA in solution even at very high NaCl or NaNO_3

Received: October 22, 2018

Revised: November 21, 2018

Published: November 21, 2018

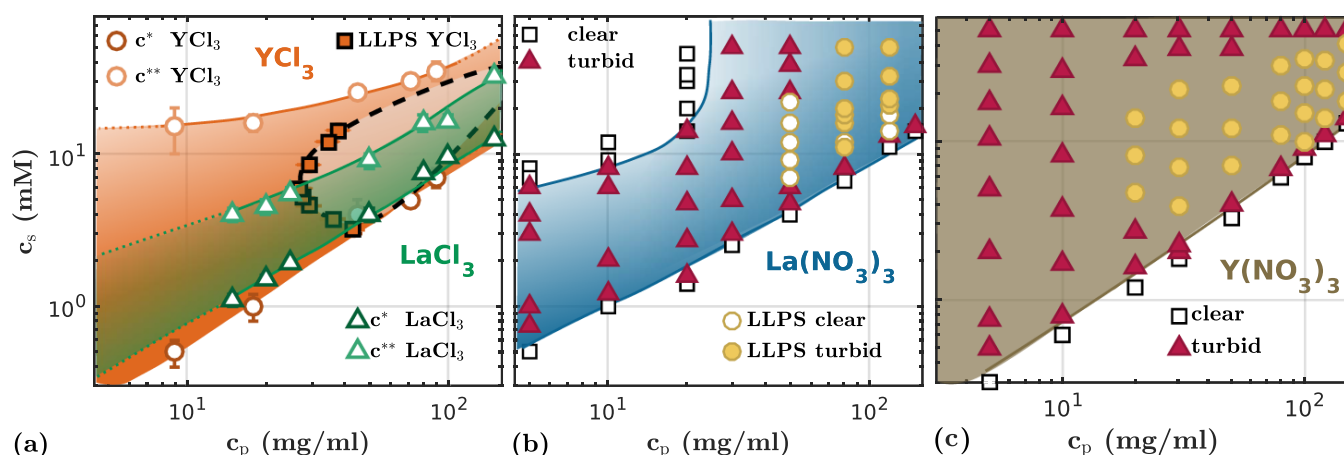


Figure 1. Experimental phase and state diagrams at room temperature for BSA with YCl_3 and LaCl_3 (a), with $\text{La}(\text{NO}_3)_3$ (b), and with $\text{Y}(\text{NO}_3)_3$ (c). For BSA with $\text{La}(\text{NO}_3)_3$ (b), above 30 mg/mL (0.45 mM) of BSA, RC disappears. The samples that show LLPS either have a clear (white circles) or a turbid (filled yellow circles) dense liquid phase.

concentrations.^{41,42} According to the Hofmeister series,^{43–45} the effect of anions on protein solubility follows the trend $\text{citrate}^{3-} > \text{SO}_4^{2-} > \text{PO}_4\text{H}^{2-} > \text{F}^- > \text{CH}_3\text{COO}^- > \text{Cl}^- > \text{Br}^- \approx \text{NO}_3^- > \text{I}^- > \text{ClO}_4^- > \text{SCN}^-$. The anion Cl^- is the most neutral one in terms of affinity to proteins and NO_3^- has a slightly higher protein affinity. In terms of destabilization of protein solutions, Cl^- is slightly stronger than NO_3^- .^{15,45} It is thus surprising to see that in the presence of a strong cation, which governs the phase behavior, these anions play an important role. The goal of this work is to present these surprisingly strong effects of monovalent anions by performing a systematic study and comparing the phase behavior of BSA in solution in the presence of four different trivalent salts. The possible mechanisms are discussed based on an enhanced Hofmeister effect.

EXPERIMENTAL SECTION

Materials and Sample Preparation. BSA (product no. A7906), LaCl_3 (product no. 298182), YCl_3 (product no. 451363), $\text{La}(\text{NO}_3)_3$ (product no. 203548, hexahydrate), and $\text{Y}(\text{NO}_3)_3$ (product no. 237957, hexahydrate) were purchased from Sigma-Aldrich and used as received. For the stock solutions, protein and salt were dissolved in degassed Milli-Q H_2O (18.2 M Ω cm conductivity). No buffer was used to avoid the effect of other co-ions. BSA has a molecular mass of 66.5 kDa and an isoelectric point of pI = 4.6. All experiments were performed at room temperature (23 ± 2 °C).

Concentrations of protein stock solutions were determined by measuring the absorbance at 280 nm using a Cary 50 UV–vis spectrophotometer (Varian Inc.) with the software Cary WinUV. The extinction coefficient of BSA is $E_{280} = 0.667$ mL/(mg cm).⁴⁶

Isothermal titration calorimetry (ITC) was used to check the effect of anions on the binding of cations to the protein. The measurements were performed with a MicroCal iTC200 instrument from Malvern Panalytical. A salt solution with a concentration c_s of 0.8 mM was titrated with 60 injections into a protein solution with a concentration c_p of 1.0 mg/mL (15 μM) at 24 °C to cover a molar ratio c_s/c_p up to 8. Titration of salt solution into pure water was performed under the same conditions. This measurement was used as a background for the correction of sample measurements.

Fourier transform infrared spectroscopy (FTIR) and circular dichroism (CD) were used to monitor the stability of the secondary protein structure in the presence of trivalent salts. An IFS 48 instrument and a VERTEX 70 instrument, both from Bruker, were used for FTIR measurements. CD measurements were performed using a J-720 spectrophotometer from JASCO Inc. For FTIR measurements, the samples were dissolved in D_2O with a protein concentration of about 20 mg/mL (0.30 mM). The samples for CD measurements were prepared in H_2O with a protein concentration of about 0.20 mg/mL (0.30 μM).

SAXS and Data Analysis. Small-angle X-ray scattering (SAXS) was employed to explore the effective protein–protein interactions in the solutions. The SAXS experiments were performed at beamline ID02 at ESRF, Grenoble, France, under the conditions that are explained in ref 31. In addition to the experimental procedure outlined there, details on beamline, q -resolution, calibration, and data reduction can be found in refs.^{47–50}

The SAXS data were analyzed using the same method as in ref 31. The data were fitted using the sticky hard sphere model which was introduced by Baxter⁵¹ and for particles with radius R reads

$$\beta U(r) = \begin{cases} \infty & r < \sigma = 2R \\ -\beta u_0 = \ln\left(\frac{12\tau\Delta}{\sigma + \Delta}\right) & \sigma < r < \sigma + \Delta \\ 0 & r > \sigma + \Delta \end{cases} \quad (1)$$

where β is equal to $1/k_B T$, τ is the stickiness parameter, and Δ is the width of the square well. The structure factor was calculated from a perturbative solution of the Percus–Yevick closure relation.^{51,52}

In the limit $\Delta \rightarrow 0$, which is used here, the reduced second virial coefficient is given by

$$\lim_{\Delta \rightarrow 0} \frac{B_2}{B_2^{\text{HS}}} = 1 - \frac{1}{4\tau} \quad (2)$$

To obtain the *reduced* second virial coefficient, B_2 is divided by the second virial coefficient for hard spheres of radius R , which is given by $B_2^{\text{HS}} = 16\pi R^3/3$. For various systems, theory

and computer simulation propose a universal value of $B_2/B_2^{\text{HS}} \approx -1.5$ at the critical point of the gas–liquid transition.^{29,53,54}

Prior to SAXS measurements, the samples were centrifuged. Only the supernatant was measured. The protein concentration in the supernatant was determined by UV–vis spectroscopy. The volume fraction in the SAXS data fit was then fixed to the corresponding value, using a value of 0.733 mL/g for the specific volume of BSA.⁵⁵ The axes r_a (axis of rotation) and r_b of the ellipsoid were fixed to 18 and 61 Å, respectively.³¹ The scattering length density (SLD) of the ellipsoid was fixed to $1.24 \times 10^{-5} \text{ \AA}^{-2}$. The background was set to an appropriate value for each curve. Moreover, Δ was fixed to 0.01σ in order to avoid artificial coupling with τ . The remaining two parameters, the SLD of the solvent and the stickiness parameter τ , were fitted. All data fitting was performed using IGOR Pro with macros provided by National Institute of Standards and Technology.⁵⁶

RESULTS AND DISCUSSION

Phase Behavior of BSA with YCl_3 , $\text{Y}(\text{NO}_3)_3$, LaCl_3 , and $\text{La}(\text{NO}_3)_3$. We first discuss the experimental phase diagram of BSA with the four salts at room temperature. Samples with protein concentrations up to 150 mg/mL (2.26 mM) and salt concentrations up to 50 mM were prepared. c^* and c^{**} can be determined either by visual inspection or by UV–vis transmission measurements as described in refs 23 and 31. Consistent with refs,^{23,31,32} Figure 1a shows the phase diagrams of BSA with the two chloride salts. The two cations, Y^{3+} and La^{3+} , lead to comparable c^* values, indicating a mainly electrostatic effect below c^* , that is, the added trivalent salts neutralize the negative surface charges of proteins. With Y^{3+} c^{**} shifts to higher values and regime II is broadened compared to La^{3+} . In addition, at room temperature, LLPS exists in a closed region inside of regime II with YCl_3 (lighter elliptical region in the YCl_3 phase diagram) but not with LaCl_3 . The orange squares in the YCl_3 phase diagram mark the c_s and c_p concentrations in the dilute phase of phase-separated samples. In order to not overload the figure, the concentrations in the dense phase are not shown. In solutions with LaCl_3 , even though there is no LLPS at room temperature, it occurs at higher temperatures. Therefore, both systems exhibit a lower critical solution temperature (LCST) phase behavior.

Figure 1b shows the state diagram for BSA in solution with $\text{La}(\text{NO}_3)_3$. Comparing this diagram with LaCl_3 in Figure 1a, it is obvious that replacing the anion Cl^- by NO_3^- leads to a significant change of the phase behavior. Although c^* is still nearly the same, c^{**} is significantly shifted upward, resulting in a broadened regime II when $\text{La}(\text{NO}_3)_3$ is used instead of LaCl_3 . At high protein concentrations, this broadening effect leads to the disappearance of c^{**} . The RC phase behavior with $\text{La}(\text{NO}_3)_3$ only exists for protein concentrations below 30 mg/mL (0.45 mM). Starting from 30 mg/mL, all samples with c_s higher than c^* are turbid. Starting from 50 mg/mL (0.75 mM) of BSA, the samples show LCST–LLPS. The dense liquid phase is either clear (white circles in Figure 1b) or turbid (yellow circles in Figure 1b). This incomplete RC behavior is also found by monitoring the protein concentration in the supernatant after centrifugation by UV–vis spectroscopy (Figure S1 in the Supporting Information). Generally, for a fixed initial protein concentration, the protein concentration in the supernatant first decreases with increasing salt concentration and after reaching a minimum increase again. For a complete RC phase behavior, the protein concentration should

return to its initial concentration in regime III. For samples with an initial BSA concentration above 50 mg/mL (0.75 mM), the protein concentrations in the supernatants do not go back to the initial value after reaching the minimum, indicating the absence of regime III, which is consistent with the findings presented in Figure 1b. Overall, based on the findings for YCl_3 , LaCl_3 , and $\text{La}(\text{NO}_3)_3$ (Figure 1), one can conclude that the change in phase behavior with $\text{La}(\text{NO}_3)_3$ is due to a stronger effective attraction between proteins when Cl^- is replaced by NO_3^- .

For BSA solutions with $\text{Y}(\text{NO}_3)_3$, no RC behavior is found any longer as no c^{**} can be identified under the current experimental conditions (Figure 1c). LLPS, however, is still observed in solutions with BSA and $\text{Y}(\text{NO}_3)_3$. The dense phases with $\text{Y}(\text{NO}_3)_3$ are all turbid. At very high salt concentration (at 50 mM and at low protein concentrations also slightly below), there is a strong whitish aggregation with $\text{Y}(\text{NO}_3)_3$. Following the results presented in Figure 1, the phase behavior of BSA with $\text{Y}(\text{NO}_3)_3$ can be rationalized by the effective attraction in this system above c^* being too strong to observe c^{**} .

The effective protein–protein interaction strength manifests itself in the RC and LLPS phase behavior. Table 1 summarizes

Table 1. Phase Behavior Overview of BSA with Four Different Trivalent Salts at Room Temperature^a

	YCl_3	$\text{Y}(\text{NO}_3)_3$	LaCl_3	$\text{La}(\text{NO}_3)_3$
RC	+		+	⊕
LLPS	+	+		+

^a⊕ indicates that the phenomenon only occurs at low protein concentrations under the current experimental conditions.

the existence and absence of RC and LLPS with all the four salts. Overall, the width of the condensed regime II and therefore the strength of the effective attraction follows the order $\text{LaCl} < 3\text{YCl}_3 < \text{La}(\text{NO}_3)_3 < \text{Y}(\text{NO}_3)_3$.

Stability of Protein Structure. Using FTIR spectroscopy and CD, the conservation of particularly the secondary protein structure was investigated in the presence of the added trivalent salts. For FTIR, the samples were prepared in D_2O with BSA concentrations of about 20 mg/mL (0.30 mM). For CD, the samples were prepared in H_2O with a low c_p around 0.20 mg/mL (3.0 μM). With chloride salts, the secondary structure of the proteins is conserved.²⁴ Representative FTIR and CD spectra of BSA solutions with $\text{La}(\text{NO}_3)_3$ are presented in Figure 2. The protein and salt concentrations c_p and c_s of the samples and the ratios between c_s and c_p are given in Table 2. The FTIR spectra in Figure 2a are normalized by the peak intensity of the amide-I band at 1650 cm^{-1} . The curves show no dramatic changes up to a $\text{La}(\text{NO}_3)_3$ concentration of 50 mM, which is the highest concentration used to prepare the samples for the phase and state diagrams in Figure 1. CD measurements (Figure 2b) were performed at the BSA concentrations of 0.20 and 0.15 mg/mL (3.0 and 2.3 μM). In order to compare the CD measurements to the FTIR measurements, it is useful to consider the c_s/c_p ratio which is listed in Table 2. Overall, neither the FTIR nor the CD measurements for BSA with $\text{La}(\text{NO}_3)_3$ show dramatic changes up to a c_s/c_p value of 170. Figures S2 and S3 in the Supporting Information show the results for BSA with $\text{Y}(\text{NO}_3)_3$. A change in the secondary structure also occurs only at high c_s/c_p .

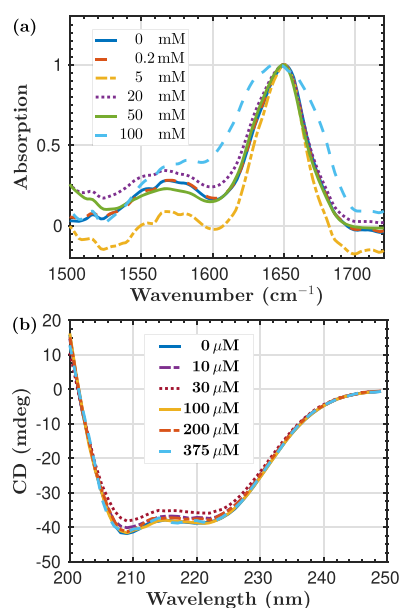


Figure 2. Protein stability in the presence of $\text{La}(\text{NO}_3)_3$ monitored by FTIR and CD. Further details on protein and salt concentrations and the ratio between them can be found in Table 2. (a) FTIR measurements for 20 mg/mL (0.30 mM) BSA with different $\text{La}(\text{NO}_3)_3$ concentrations. The spectra were normalized by the peak value at 1650 cm^{-1} . (b) CD measurements for 0.20 and 0.15 mg/mL BSA with different $\text{La}(\text{NO}_3)_3$ concentrations. Both FTIR and CD show that for BSA with $\text{La}(\text{NO}_3)_3$, the secondary structure is conserved up to high $\text{La}(\text{NO}_3)_3$ concentrations.

Table 2. Protein and Salt Concentrations and the Ratio between Them for the FTIR and CD Measurements

FTIR	0	0.2	5	20	50	100	c_s (mM)
	20	20	20	20	20	20	c_p (mg/mL)
	0	0.67	17	67	170	330	c_s/c_p
CD	0	10	30	100	200	375	c_s (μM)
	0.20	0.20	0.20	0.20	0.20	0.15	c_p (mg/mL)
	0	3.3	10	33	67	170	c_s/c_p

Therefore, under the experimental conditions in Figure 1, proteins are stable and their secondary structure is preserved.

Effects of Anions on Cation Binding Characterized by ITC. ITC was used to characterize the effect of anions on cation binding to BSA. The direct result of an ITC measurement is the heat flow due to the binding process. Figure 3 shows the results for BSA with both pairs of salts. The overall heat flow is positive for all measurements, which means that the cation binding is an endothermic and thus an entropy-driven process.³² For both cations, the ITC spectra with the two different anions overlap within the experimental error. The integral total binding enthalpy ΔH values are 27 ± 2 and 22 ± 2 kcal/mol for yttrium and lanthanum salts, respectively. This result suggests that the replacing of anions does not significantly influence the cation binding process to BSA itself.

Effective Protein–Protein Interactions Characterized by SAXS. Representative SAXS data with model fitting for samples with 85 mg/mL (1.28 mM) of BSA are presented in Figure 4. At low salt concentrations, the effective protein–protein interactions are dominated by electrostatic repulsion. A strong correlation peak is visible in the SAXS profiles. In this region of the phase diagram (regime I), the solutions are clear. By increasing the salt concentration, the low q intensity

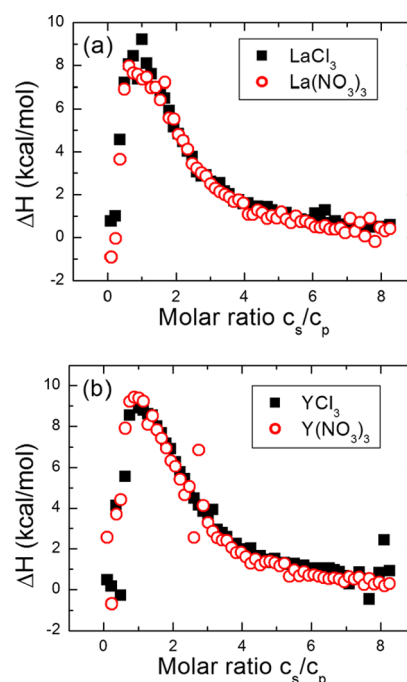


Figure 3. ITC spectra for cation binding to BSA. (a) LaCl_3 and $\text{La}(\text{NO}_3)_3$ and (b) YCl_3 and $\text{Y}(\text{NO}_3)_3$. Salt solutions of 0.8 mM were titrated into a solution of 1.0 mg/mL (15 μM) of BSA.

increases, indicating the reduction of repulsion. By further increasing the salt concentration, the interactions become attractive, and the low q intensity reaches a maximum at about 9–10 mM $\text{La}(\text{NO}_3)_3$ (Figure 4a). For c_s in the range between 10 and 20 mM, the low q intensity decreases (Figure 4b) and then increases again up to 50 mM (Figure 4c).

Starting from 6 mM $\text{La}(\text{NO}_3)_3$, the SAXS data were fitted using an ellipsoid form factor combined with a sticky hard sphere potential.⁵¹ In Figure 4, the fits are superimposed on the data as solid black lines. The resulting B_2/B_2^{HS} values are shown in Figure 5a and the inverse of the intensities at low q , $1/I(q \rightarrow 0)$, is shown in Figure 5b. The data are compared to the results for BSA with LaCl_3 and BSA with YCl_3 .^{31,57}

The B_2/B_2^{HS} curves first decrease sharply in a similar manner for all the three salts. Then, after reaching a minimum, the B_2/B_2^{HS} curves increase again but with a trend strongly depending on the salt. The steepness of this increase decreases from LaCl_3 to YCl_3 to $\text{La}(\text{NO}_3)_3$. In the case of $\text{La}(\text{NO}_3)_3$, the values remain almost constant. This explains the absence of c^{**} at high protein concentrations. The values of B_2/B_2^{HS} for BSA with LaCl_3 are the highest and the ones with $\text{La}(\text{NO}_3)_3$ are the lowest, in good agreement with the phase behavior in Figure 1. These results of B_2/B_2^{HS} in Figure 5a clearly show that replacing Cl^- by NO_3^- enhances the effective attractions between BSA molecules.

We suppose that the reason for the nonsymmetric change is the screening effect of the co-ion, Cl^- or NO_3^- . The increasing amount of co-ions screens the effective surface charge of the proteins. Fujihara and Akiyama studied the attractive interaction between macroanions mediated by divalent cations and observed a similar asymmetric trend of the effective interaction potential as a function of cation concentration.^{58,59} The stronger effective attraction which is thought to be due to the higher protein affinity of NO_3^- leads to a stronger asymmetry with $\text{La}(\text{NO}_3)_3$ than with LaCl_3 or YCl_3 .

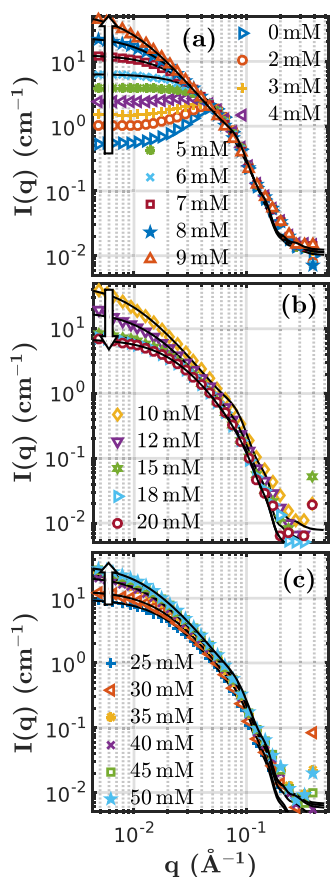


Figure 4. SAXS data with model fits for samples with 85 mg/mL (1.28 mM) of BSA and different concentrations of $\text{La}(\text{NO}_3)_3$. (a) Approaching c^* and slightly above c^* , the scattering intensity at low q increases with increasing salt concentration. Starting from 6 mM $\text{La}(\text{NO}_3)_3$, the data were fitted using a sticky hard sphere potential (solid black lines). (b) Starting from 10 mM, the samples phase-separated. The scattering intensity at low q decreases. (c) Still in the phase separation regime, which extends up to 50 mM for $\text{La}(\text{NO}_3)_3$, the scattering intensity at low q increases again.

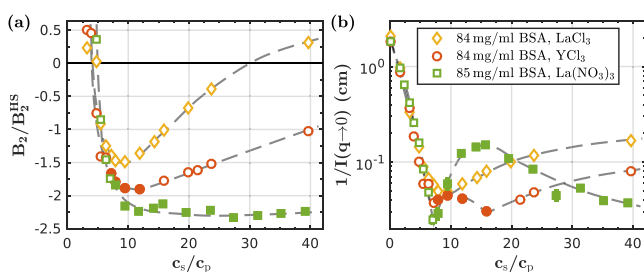


Figure 5. (a) Reduced second virial coefficients, B_2/B_2^{HS} , calculated from the SAXS data analysis for $c_s \geq c^*$. Filled symbols indicate samples exhibiting LLPS. Dashed lines are guides to the eye. (b) Inverse scattering intensity at $q \rightarrow 0$ (mean of the first three to five data points) from the full SAXS data set.

Without imposing any model, the scattering at low q , $I(q \rightarrow 0)$, as a function of c_s/c_p (Figure 5b) shows the same trends of the effective interaction as B_2/B_2^{HS} does. In the rest of this section, $I(q \rightarrow 0)$ is abbreviated as $I(0)$ for simplicity. It is related to compressibility χ_T ⁶⁰

$$I(0) \propto S(q \rightarrow 0) = k_B T \rho \chi_T \quad (3)$$

The compressibility χ_T diverges at the spinodal line.⁶⁰ When the coexisting densities differ hardly, the binodal line is close to the spinodal line. In this case, χ_T becomes large and $1/I(0)$ becomes small. In addition, the virial expansion gives^{4,60}

$$1/S(q \rightarrow 0) = 1 + 2B_2\rho + \dots \quad (4)$$

Without LLPS, the protein concentration $c_p \propto \rho$ in the measured dilute phase remains constant, which means that $1/I(0)$ follows the trend of B_2/B_2^{HS} . When LLPS occurs, the variation of c_p in the measured dilute phase leads to the difference between the $1/I(0)$ curve and the B_2/B_2^{HS} curve. Note that because of the phase equilibrium, the B_2/B_2^{HS} value is the same in the corresponding dense and dilute phases.^{54,61,62}

The experimental results on the microscopic interactions reflect the macroscopic phase behavior and vice versa. This can be seen by comparing $1/I(0)$ in Figure 5b with the RC and LLPS phase behavior shown in Figure 1. For samples with LaCl_3 , without LLPS binodal, $1/I(0)$ decreases and then increases and follows the trends of B_2/B_2^{HS} . For samples with YCl_3 and $\text{La}(\text{NO}_3)_3$, the existence of the LLPS binodal changes the behavior of $1/I(0)$. In the LLPS region, there is an additional increase and decrease. Close to the critical points of LLPS $1/I(0)$ is minimal, as there the compressibility diverges. Note that for $\text{La}(\text{NO}_3)_3$, the LLPS region extends up to $c_s/c_p \geq 40$. Apart from this additional increase and decrease, $1/I(0)$ follows the trends of B_2/B_2^{HS} .

Discussion on the Role of Anions on the Phase Behavior. The strong effects of the anions on the reentrant phase behavior in protein solutions deserve further discussion. The RC phase behavior in protein solutions induced by trivalent salts has been explained by the effective charge inversion of proteins.^{23–25} Thus, the cation binding and bridging has been considered as the main source of attraction. In fact, an ion-activated patchy colloid model has been proposed to rationalize the experimental results.⁶³ Therefore, an intuitive assumption would be that replacing Cl^- by NO_3^- leads to an enhanced cation binding affinity. However, the ITC curves (Figure 3) are essentially the same for both anions used, indicating no difference in the cation binding process. This leads to the assumption that the increasing attraction is due to the anion effects on the protein–cation complex. The effective interactions between the complexes may include electrostatic interactions (binding and other nonspecific interactions via charged surface residues) and hydrophobic interactions. Thus, the results suggest that this overall effect is sensitive to the protein affinity of the anions.

In the Hofmeister series, the anions Cl^- and NO_3^- are close to each other, and Cl^- has been considered a rather weak or neutral anion in terms of its affinity to proteins. NO_3^- has a slightly stronger affinity to the protein surface according to the Hofmeister series.⁴⁵ We suppose that by increasing the trivalent salt concentration, more cations bind and turn the protein–cation complex positive, and the stronger affinity of NO_3^- to the protein surface decreases the surface charge of the protein more strongly than Cl^- does. Consequently, the samples remain in an aggregated state because of a stronger effective attraction.

Another possible contribution to this experimental observation could be the complex formation of cations with anions, which competes with the binding of the cation to the carboxyl groups on the protein surface. However, studies have shown that the anion–rare earth element complex formation becomes important only at very high salt concentrations above 0.5

M.^{64–66} Therefore, the effects of complex formation should be rather weak under the current experimental conditions.

Normally, Hofmeister effects become important at salt concentrations well above 100 mM.^{43–45} In the work presented here, the anions show significant effects on interactions (Figure 5) and phase behavior already at concentrations below 100 mM (Figure 1). Understanding these enhanced Hofmeister effects needs further insights into the anion–protein interactions on the molecular level. Fox et al., for example, studied interactions between Hofmeister anions and a binding pocket of a Zn²⁺ cofactor protein.⁶⁷ Their results indicate that the Hofmeister anions form inner sphere ion pairs with the protein. Importantly, they found that the association of anions with Zn²⁺ in the binding pocket of a protein leads to rearrangement of water up to a few layers (8 Å) away from the anion surfaces, indicating a strong entropic effect. Furthermore, this study reveals another important difference between Cl[−] and NO₃[−];⁶⁷ that is, although the binding free energy only slightly decreases from Cl[−] to NO₃[−], the contributions from enthalpy and entropy are markedly different between these two anions. The monoatomic anion Cl[−] causes a small entropy change upon binding, whereas NO₃[−] induces a strong entropy change upon binding. Therefore, the enthalpy change has to be even stronger to compensate for the entropy loss. How exactly these differences between anions modify the protein interactions in the presence of trivalent cations is still an open question, which requires studies on the atomic level at the binding sites for both cations and anions.

CONCLUSIONS

In summary, we have characterized the RC phase behavior and effective interactions in protein solutions in the presence of trivalent salts focusing on the effects of the anions Cl[−] versus NO₃[−]. We found that replacing Cl[−] by NO₃[−] leads to a significantly enhanced effective attraction. This enhanced attraction manifests itself at low protein concentrations in a broadening and, at high protein concentrations, in the disappearance of regime II. Overall, the width of the condensed regime II and hence also the strength of the effective attraction follows the order LaCl₃ < YCl₃ < La(NO₃)₃ < Y(NO₃)₃. Both chloride salts show RC. At room temperature, LLPS is present with YCl₃ but not with LaCl₃ because of a stronger effective attraction with YCl₃. With both nitrate salts the effective attraction is strong enough to induce LLPS. Partial RC is found with La(NO₃)₃ and no RC is found with Y(NO₃)₃ because of a stronger effective attraction with the nitrate salts.

This strong effect of anions is further supported by the effective protein–protein interactions characterized by SAXS. Using a sticky hard sphere model, the attractive interactions are quantitatively described by the reduced second virial coefficient, B_2/B_2^{HS} . In addition, $1/I(q \rightarrow 0)$ as a function of c_s/c_p provides a qualitative description of interaction, compressibility, and LLPS. The results demonstrate that the nitrate salts induce a stronger effective attraction than the chloride salts, which explains the observed phase behavior.

FTIR and CD measurements demonstrate that the protein structures are conserved under the experimental conditions. Therefore, significant effects of partial protein unfolding can be ruled out. In contrast to the marked changes in phase behavior and effective protein–protein interactions characterized by SAXS, the protein–cation binding profiles recorded by ITC

indicate that replacing Cl[−] by NO₃[−] has no significant impact on the cation binding process. The strong anion effect may thus be explained by an enhanced Hofmeister effect. The stronger protein affinity of NO₃[−] compared to Cl[−] influences the charge state of the proteins and results in an enhanced attraction between the protein–cation complexes.

ASSOCIATED CONTENT

Supporting Information

The Supporting Information is available free of charge on the ACS Publications website at DOI: 10.1021/acs.jpcc.8b10268.

BSA concentration in the supernatant with increasing La(NO₃)₃ concentration and further FTIR and CD spectra for BSA with LaCl₃ and Y(NO₃)₃ (PDF)

AUTHOR INFORMATION

Corresponding Author

*E-mail: fajun.zhang@uni-tuebingen.de.

ORCID

Michal K. Braun: 0000-0002-9642-7492

Olga Matsarskaia: 0000-0002-7293-7287

Felix Roosen-Runge: 0000-0001-5106-4360

Roland Roth: 0000-0001-6271-7646

Fajun Zhang: 0000-0001-7639-8594

Present Address

[†]Austrian SAXS beamline, ELETTRA Sincrotrone, Trieste, Italy, Outstation of the Institut für Anorganische Chemie, Technische Universität Graz, Streymayrgasse 9/V, 8010 Graz.

Notes

The authors declare no competing financial interest.

ACKNOWLEDGMENTS

We thank S. Da Vela for valuable discussions. Furthermore, we acknowledge the contributions from P. Christodoulou, N. Scheffczyk, and S. Schönberg in this project. We thank Prof. T. Stehle and N. Jaspert (Tübingen) for sharing their laboratory resources. O.M. gratefully acknowledges a PhD fellowship by Studienstiftung des deutschen Volkes. We gratefully acknowledge the allocation of beamline from ESRF and access to the PSCM lab in Grenoble, France. Furthermore, this work was supported by the DFG.

REFERENCES

- (1) Anderson, V. J.; Lekkerkerker, H. N. W. Insights into Phase Transition Kinetics from Colloid Science. *Nature* **2002**, *416*, 811–815.
- (2) Piazza, R. Protein Interactions and Association: An Open Challenge for Colloid Science. *Curr. Opin. Colloid Interface Sci.* **2004**, *8*, 515–522.
- (3) ten Wolde, P. R.; Frenkel, D. Enhancement of Protein Crystal Nucleation by Critical Density Fluctuations. *Science* **1997**, *277*, 1975–1978.
- (4) Gunton, J.; Shiryayev, A.; Pagan, D. *Protein Condensation: Kinetic Pathways to Crystallization and Disease*; Cambridge University Press, 2007.
- (5) Brangwynne, C. P.; Eckmann, C. R.; Courson, D. S.; Rybarska, A.; Hoeghe, C.; Gharakhani, J.; Julicher, F.; Hyman, A. A. Germline P Granules are Liquid Droplets that Localize by Controlled Dissolution/Condensation. *Science* **2009**, *324*, 1729–1732.
- (6) Li, Y.; Lubchenko, V.; Vorontsova, M. A.; Filobelo, L.; Vekilov, P. G. Ostwald-Like Ripening of the Anomalous Mesoscopic Clusters in Protein Solutions. *J. Phys. Chem. B* **2012**, *116*, 10657–10664.

- (7) Durbin, S. D.; Feher, G. Protein Crystallization. *Annu. Rev. Phys. Chem.* **1996**, *47*, 171–204.
- (8) Galkin, O.; Vekilov, P. G. Are Nucleation Kinetics of Protein Crystals Similar to Those of Liquid Droplets? *J. Am. Chem. Soc.* **2000**, *122*, 156–163.
- (9) Benedek, G. B. Cataract as a Protein Condensation Disease: the Proctor Lecture. *Invest. Ophthalmol. Visual Sci.* **1997**, *38*, 1911–1921.
- (10) Piazza, R. Interactions and Phase Transitions in Protein Solutions. *Curr. Opin. Colloid Interface Sci.* **2000**, *5*, 38–43.
- (11) Sear, R. Interactions in Protein Solutions. *Curr. Opin. Colloid Interface Sci.* **2006**, *11*, 35–39.
- (12) Muschol, M.; Rosenberger, F. Liquid–Liquid Phase Separation in Supersaturated Lysozyme Solutions and Associated Precipitate Formation/Crystallization. *J. Chem. Phys.* **1997**, *107*, 1953–1962.
- (13) Curtis, R. A.; Blanch, H. W.; Prausnitz, J. M. Calculation of Phase Diagrams for Aqueous Protein Solutions. *J. Phys. Chem. B* **2001**, *105*, 2445–2452.
- (14) Curtis, R. A.; Prausnitz, J. M.; Blanch, H. W. Protein–Protein and Protein–Salt Interactions in Aqueous Protein Solutions Containing Concentrated Electrolytes. *Biotechnol. Bioeng.* **1998**, *57*, 11–21.
- (15) Collins, K. Ions from the Hofmeister Series and Osmolytes: Effects on Proteins in Solution and in the Crystallization Process. *Methods* **2004**, *34*, 300–311.
- (16) Rosenbaum, D.; Zamora, P. C.; Zukoski, C. F. Phase Behavior of Small Attractive Colloidal Particles. *Phys. Rev. Lett.* **1996**, *76*, 150–153.
- (17) Muschol, M.; Rosenberger, F. Interactions in Undersaturated and Supersaturated Lysozyme Solutions: Static and Dynamic Light Scattering Results. *J. Chem. Phys.* **1995**, *103*, 10424.
- (18) Tardieu, A.; Le Verge, A.; Malfois, M.; Bonneté, F.; Finet, S.; Riès-Kautt, M.; Belloni, L. Proteins in Solution: From X-Ray Scattering Intensities to Interaction Potentials. *J. Cryst. Growth* **1999**, *196*, 193–203.
- (19) Velev, O. D.; Kaler, E. W.; Lenhoff, A. M. Protein Interactions in Solution Characterized by Light and Neutron Scattering: Comparison of Lysozyme and Chymotrypsinogen. *Biophys. J.* **1998**, *75*, 2682–2697.
- (20) Stradner, A.; Sedgwick, H.; Cardinaux, F.; Poon, W. C. K.; Egelhaaf, S. U.; Schurtenberger, P. Equilibrium Cluster Formation in Concentrated Protein Solutions and Colloids. *Nature* **2004**, *432*, 492–495.
- (21) Thomson, J. A.; Schurtenberger, P.; Thurston, G. M.; Benedek, G. B. Binary Liquid Phase Separation and Critical Phenomena in a Protein/Water Solution. *Proc. Natl. Acad. Sci. U.S.A.* **1987**, *84*, 7079–7083.
- (22) Liu, Y.; Fratini, E.; Baglioni, P.; Chen, W.-R.; Chen, S.-H. Effective Long-Range Attraction between Protein Molecules in Solutions Studied by Small Angle Neutron Scattering. *Phys. Rev. Lett.* **2005**, *95*, 118102.
- (23) Zhang, F.; Skoda, M. W. A.; Jacobs, R. M. J.; Zorn, S.; Martin, R. A.; Martin, C. M.; Clark, G. F.; Weggler, S.; Hildebrandt, A.; Kohlbacher, O.; et al. Reentrant Condensation of Proteins in Solution Induced by Multivalent Counterions. *Phys. Rev. Lett.* **2008**, *101*, 148101.
- (24) Zhang, F.; Weggler, S.; Ziller, M. J.; Ianeselli, L.; Heck, B. S.; Hildebrandt, A.; Kohlbacher, O.; Skoda, M. W. A.; Jacobs, R. M. J.; Schreiber, F. Universality of Protein Reentrant Condensation in Solution Induced by Multivalent Metal Ions. *Proteins: Struct., Funct., Bioinf.* **2010**, *78*, 3450–3457.
- (25) Zhang, F.; Roosen-Runge, F.; Sauter, A.; Wolf, M.; Jacobs, R. M. J.; Schreiber, F. Reentrant Condensation, Liquid-Liquid Phase Separation and Crystallization in Protein Solutions Induced by Multivalent Metal Ions. *Pure Appl. Chem.* **2014**, *86*, 191–202.
- (26) Roosen-Runge, F.; Heck, B. S.; Zhang, F.; Kohlbacher, O.; Schreiber, F. Interplay of pH and Binding of Multivalent Metal Ions: Charge Inversion and Reentrant Condensation in Protein Solutions. *J. Phys. Chem. B* **2013**, *117*, 5777–5787.
- (27) Jordan, E.; Roosen-Runge, F.; Leibfarth, S.; Zhang, F.; Sztucki, M.; Hildebrandt, A.; Kohlbacher, O.; Schreiber, F. Competing Salt Effects on Phase Behavior of Protein Solutions: Tailoring of Protein Interaction by the Binding of Multivalent Ions and Charge Screening. *J. Phys. Chem. B* **2014**, *118*, 11365–11374.
- (28) Zhang, F.; Roth, R.; Wolf, M.; Roosen-Runge, F.; Skoda, M. W. A.; Jacobs, R. M. J.; Sztucki, M.; Schreiber, F. Charge-Controlled Metastable Liquid-Liquid Phase Separation in Protein Solutions as a Universal Pathway towards Crystallization. *Soft Matter* **2012**, *8*, 1313–1316.
- (29) Wolf, M.; Roosen-Runge, F.; Zhang, F.; Roth, R.; Skoda, M. W. A.; Jacobs, R. M. J.; Sztucki, M.; Schreiber, F. Effective Interactions in Protein–Salt Solutions Approaching Liquid–Liquid Phase Separation. *J. Mol. Liq.* **2014**, *200*, 20–27.
- (30) Zhang, F. Nonclassical Nucleation Pathways in Protein Crystallization. *J. Phys.: Condens. Matter* **2017**, *29*, 443002.
- (31) Braun, M. K.; Wolf, M.; Matsarskaia, O.; Da Vela, S.; Roosen-Runge, F.; Sztucki, M.; Roth, R.; Zhang, F.; Schreiber, F. Strong Isotope Effects on Effective Interactions and Phase Behavior in Protein Solutions in the Presence of Multivalent Ions. *J. Phys. Chem. B* **2017**, *121*, 1731–1739.
- (32) Matsarskaia, O.; Braun, M. K.; Roosen-Runge, F.; Wolf, M.; Zhang, F.; Roth, R.; Schreiber, F. Cation-Induced Hydration Effects Cause Lower Critical Solution Temperature Behavior in Protein Solutions. *J. Phys. Chem. B* **2016**, *120*, 7731–7736.
- (33) Zhang, F.; Zocher, G.; Sauter, A.; Stehle, T.; Schreiber, F. Novel Approach to Controlled Protein Crystallization through Ligandation of Yttrium Cations. *J. Appl. Crystallogr.* **2011**, *44*, 755–762.
- (34) Zhang, F.; Roosen-Runge, F.; Sauter, A.; Roth, R.; Skoda, M. W. A.; Jacobs, R. M. J.; Sztucki, M.; Schreiber, F. The Role of Cluster Formation and Metastable Liquid-Liquid Phase Separation in Protein Crystallization. *Faraday Discuss.* **2012**, *159*, 313–325.
- (35) Sauter, A.; Roosen-Runge, F.; Zhang, F.; Lotze, G.; Jacobs, R. M. J.; Schreiber, F. Real-Time Observation of Nonclassical Protein Crystallization Kinetics. *J. Am. Chem. Soc.* **2015**, *137*, 1485–1491.
- (36) Sauter, A.; Roosen-Runge, F.; Zhang, F.; Lotze, G.; Feoktystov, A.; Jacobs, R. M. J.; Schreiber, F. On the Question of Two-Step Nucleation in Protein Crystallization. *Faraday Discuss.* **2015**, *179*, 41–58.
- (37) Soraruf, D.; Roosen-Runge, F.; Grimaldo, M.; Zanini, F.; Schweins, R.; Seydel, T.; Zhang, F.; Roth, R.; Oettel, M.; Schreiber, F. Protein Cluster Formation in Aqueous Solution in the Presence of Multivalent Metal Ions - A Light Scattering Study. *Soft Matter* **2014**, *10*, 894–902.
- (38) Da Vela, S.; Braun, M. K.; Dörr, A.; Greco, A.; Möller, J.; Fu, Z.; Zhang, F.; Schreiber, F. Kinetics of Liquid–Liquid Phase Separation in Protein Solutions Exhibiting LCST Phase Behavior Studied by Time-Resolved USAXS and VSANS. *Soft Matter* **2016**, *12*, 9334–9341.
- (39) Da Vela, S.; Roosen-Runge, F.; Skoda, M. W. A.; Jacobs, R. M. J.; Seydel, T.; Frielinghaus, H.; Sztucki, M.; Schweins, R.; Zhang, F.; Schreiber, F. Effective Interactions and Colloidal Stability of Bovine γ -Globulin in Solution. *J. Phys. Chem. B* **2017**, *121*, 5759–5769.
- (40) Matsarskaia, O.; Roosen-Runge, F.; Lotze, G.; Möller, J.; Mariani, A.; Zhang, F.; Schreiber, F. Tuning phase transitions of aqueous protein solutions by multivalent cations. *Phys. Chem. Chem. Phys.* **2018**, *20*, 27214–27225.
- (41) Zhang, F.; Skoda, M. W. A.; Jacobs, R. M. J.; Martin, R. A.; Martin, C. M.; Schreiber, F. Protein Interactions Studied by SAXS: Effect of Ionic Strength and Protein Concentration for BSA in Aqueous Solutions. *J. Phys. Chem. B* **2007**, *111*, 251–259.
- (42) Zhang, F.; Roosen-Runge, F.; Skoda, M. W. A.; Jacobs, R. M. J.; Wolf, M.; Callow, P.; Frielinghaus, H.; Pipich, V.; Prévost, S.; Schreiber, F. Hydration and Interactions in Protein Solutions Containing Concentrated Electrolytes Studied by Small-Angle Scattering. *Phys. Chem. Chem. Phys.* **2012**, *14*, 2483–2493.
- (43) Hofmeister, F. Zur Lehre von der Wirkung der Salze. *Schmiedeb. Arch. für Exp. Pathol. Pharmacol.* **1888**, *24*, 247–260.

- (44) Lo Nostro, P.; Ninham, B. W. Hofmeister Phenomena: An Update on Ion Specificity in Biology. *Chem. Rev.* **2012**, *112*, 2286–2322.
- (45) Okur, H. I.; Hladílková, J.; Rembert, K. B.; Cho, Y.; Heyda, J.; Dzubiel, J.; Cremer, P. S.; Jungwirth, P. Beyond the Hofmeister Series: Ion-Specific Effects on Proteins and Their Biological Functions. *J. Phys. Chem. B* **2017**, *121*, 1997–2014.
- (46) Sober, H. A. *CRC Handbook of Biochemistry: Selected Data for Molecular Biology*; The Chemical Rubber Co.: Cleveland, Ohio, 1970.
- (47) Narayanan, T.; Diat, O.; Bösecke, P. SAXS and USAXS on the High Brilliance Beamline at the ESRF. *Nucl. Instrum. Methods Phys. Res., Sect. A* **2001**, *467–468*, 1005–1009.
- (48) *Soft Matter Characterization*; Borsali, R., Pecora, R., Eds.; Springer: New York, 2008; Chapter 17.
- (49) Narayanan, T.; Sztucki, M.; Van Vaerenbergh, P.; Léonardon, J.; Gorini, J.; Claustre, L.; Sever, F.; Morse, J.; Boesecke, P. A Multipurpose Instrument for Time-Resolved Ultra Small-Angle and Coherent X-Ray Scattering. *J. Appl. Crystallogr.* **2018**, *51*, 1511–1524.
- (50) Ianeselli, L.; Zhang, F.; Skoda, M. W. A.; Jacobs, R. M. J.; Martin, R. A.; Callow, S.; Prévost, S.; Schreiber, F. Protein-Protein Interactions in Ovalbumin Solutions Studied by Small-Angle Scattering: Effect of Ionic Strength and the Chemical Nature of Cations. *J. Phys. Chem. B* **2010**, *114*, 3776–3783.
- (51) Baxter, R. J. Percus–Yevick Equation for Hard Spheres with Surface Adhesion. *J. Chem. Phys.* **1968**, *49*, 2770–2774.
- (52) Menon, S. V. G.; Manohar, C.; Rao, K. S. A New Interpretation of the Sticky Hard Sphere Model. *J. Chem. Phys.* **1991**, *95*, 9186–9190.
- (53) Vliegenthart, G. A.; Lekkerkerker, H. N. W. Predicting the Gas–Liquid Critical Point from the Second Virial Coefficient. *J. Chem. Phys.* **2000**, *112*, 5364–5369.
- (54) Noro, M. G.; Frenkel, D. Extended Corresponding-States Behavior for Particles with Variable Range Attractions. *J. Chem. Phys.* **2000**, *113*, 2941–2944.
- (55) Putnam, F. *The Plasma Proteins: Structure, Function and Genetic Control*, 2nd ed.; Academic Press: New York, 1975; Vol. 1, pp 141–147.
- (56) Kline, S. R. Reduction and Analysis of SANS and USANS Data Using IGOR Pro. *J. Appl. Crystallogr.* **2006**, *39*, 895–900.
- (57) Fries, M. R.; Stopper, D.; Braun, M. K.; Hinderhofer, A.; Zhang, F.; Jacobs, R. M. J.; Skoda, M. W. A.; Hansen-Goos, H.; Roth, R.; Schreiber, F. Multivalent-Ion-Activated Protein Adsorption Reflecting Bulk Reentrant Behavior. *Phys. Rev. Lett.* **2017**, *119*, 228001.
- (58) Fujihara, S.; Akiyama, R. Attractive Interaction between Macroanions Mediated by Multivalent Cations in Biological Fluids. *J. Mol. Liq.* **2014**, *200*, 89–94.
- (59) Akiyama, R.; Sakata, R. An Integral Equation Study of Reentrant Behavior in Attractive Interactions between Like-Charged Macroions Immersed in an Electrolyte Solution. *J. Phys. Soc. Jpn.* **2011**, *80*, 123602.
- (60) Hansen, J.-P.; McDonald, I. R. *Theory of Simple Liquids*, 3rd ed.; Academic Press Amsterdam, 2006.
- (61) Stradner, A.; Cardinaux, F.; Schurtenberger, P. A Small-Angle Scattering Study on Equilibrium Clusters in Lysozyme Solutions. *J. Phys. Chem. B* **2006**, *110*, 21222–21231.
- (62) Platten, F.; Hansen, J.; Wagner, D.; Egelhaaf, S. U. Second Virial Coefficient As Determined from Protein Phase Behavior. *J. Phys. Chem. Lett.* **2016**, *7*, 4008–4014.
- (63) Roosen-Runge, F.; Zhang, F.; Schreiber, F.; Roth, R. Ion-Activated Attractive Patches as a Mechanism for Controlled Protein Interactions. *Sci. Rep.* **2014**, *4*, 7016.
- (64) Wood, S. A. The aqueous geochemistry of the rare-earth elements and yttrium. *Chem. Geol.* **1990**, *82*, 159–186.
- (65) Wood, S. A. The aqueous geochemistry of the rare-earth elements and yttrium. *Chem. Geol.* **1990**, *88*, 99–125.
- (66) Rudolph, W. W.; Irmer, G. Hydration and Ion Pair Formation in Aqueous Y^{3+} -Salt Solutions. *Dalton Trans.* **2015**, *44*, 18492–18505.
- (67) Fox, J. M.; Kang, K.; Sherman, W.; Héroux, A.; Sastry, G. M.; Baghbanzadeh, M.; Lockett, M. R.; Whitesides, G. M. Interactions between Hofmeister Anions and the Binding Pocket of a Protein. *J. Am. Chem. Soc.* **2015**, *137*, 3859–3866.